Delta spike P681R mutation enhances SARS-CoV-2 fitness over Alpha variant

Yang Liu[1,2,*], Jianying Liu[2,3,4,*], Bryan A. Johnson[4], Hongjie Xia[1], Zhiqiang Ku[5], Craig Schindewolf[2,3,4], Steven G. Widen[1], Zhiqiang An[5], Scott C. Weaver[2,3,4], Vineet D. Menachery[2,3,4], Xuping Xie[1#], and Pei-Yong Shi[1,2,3,#]

[1]Department of Biochemistry and Molecular Biology, University of Texas Medical Branch, Galveston TX, USA

[2]Institute for Human Infections and Immunity, University of Texas Medical Branch, Galveston TX, USA

[3]World Reference Center for Emerging Viruses and Arboviruses, University of Texas Medical Branch, Galveston TX, USA

[4]Department of Microbiology and Immunology, University of Texas Medical Branch, Galveston TX, USA

[5]Texas Therapeutics Institute, Brown Foundation Institute of Molecular Medicine, The University of Texas Health Science Center at Houston, Houston, TX 77030, USA

*YL and JL made equal contributions to the study

[#]Correspondence: X.X. (xuxie@UTMB.edu) or P.-Y.S. (peshi@UTMB.edu)

Abstract

SARS-CoV-2 Delta variant has rapidly replaced the Alpha variant around the world. The mechanism that drives this global replacement has not been defined. Here we report that Delta spike mutation P681R plays a key role in the Alpha-to-Delta variant replacement. In a replication competition assay, Delta SARS-CoV-2 efficiently outcompeted the Alpha variant in human lung epithelial cells and primary human airway tissues. Delta SARS-CoV-2 bearing the Alpha-spike glycoprotein replicated less efficiently than the wild-type Delta variant, suggesting the importance of Delta spike in enhancing viral replication. The Delta spike has accumulated mutation P681R located at a furin cleavage site that separates the spike 1 (S1) and S2 subunits. Reverting the P681R mutation to wild-type P681 significantly reduced the replication

of Delta variant, to a level lower than the Alpha variant. Mechanistically, the Delta P681R mutation enhanced the cleavage of the full-length spike to S1 and S2, leading to increased infection via cell surface entry. In contrast, the Alpha spike also has a mutation at the same amino acid (P681H), but the spike cleavage from purified Alpha virions was reduced compared to the Delta spike. Collectively, our results indicate P681R as a key mutation in enhancing Delta variant replication via increased S1/S2 cleavage. Spike mutations that potentially affect furin cleavage efficiency must be closely monitored for future variant surveillance.

Introduction

The continuous emergence of new variants of severe acute respiratory syndrome coronavirus 2 (SARS-CoV-2) poses the greatest threat to pandemic control, vaccine effectiveness, therapeutic efficacy, and surveillance. Since its emergence in late 2019, mutations have unceasingly emerged in the circulating viruses, leading to variants with enhanced transmissibility, evasion of therapeutic antibodies, and breakthrough infections in vaccinated individuals.[1-6] Since the viral spike glycoprotein is responsible for binding to the human cellular receptor angiotensin-converting enzyme (ACE2), many mutations have accumulated in the spike gene with the potential to alter viral fitness or to escape immunity. The variants have emerged from different geographic regions and, depending on their biological properties, spread to other regions. The World Health Organization (WHO) has classified variants as “variants of concern” (*i.e.*, Alpha, Beta, Gamma, and Delta) and “variants of interest” (*i.e.*, Eta, Iota, Kappa, and Lambda).[7] The Alpha variant was first identified in the United Kingdom in September 2020 and subsequently became dominant in many parts of the world. Afterwards, the Delta variant emerged in India in October 2020 and has now spread to over 119 countries, displacing the Alpha variant globally.[7,8] From May 2 to July 31 of 2021, the prevalence of the Delta variant in the USA had increased from 1.3% to 94.4%, whereas the

prevalence of the Alpha variant had decreased from 70% to 2.4%. More seriously, the Delta variant has been associated with increased transmissibility, disease severity, and breakthrough infections in vaccinated individuals.[5,9-11] The mutation(s) that have driven the explosive spread of the Delta variant and its displacement of the Alpha variant remain to be defined. In this study, we used a reverse genetic approach to identify the molecular determinant(s) for the enhanced fitness of Delta variant and its dominance over the Alpha variant.

Results

We constructed infectious cDNA clones for the Alpha (GISAIS ID: EPI_ISL_999340) and Delta (GISAIS ID: EPI_ISL_2100646) SARS-CoV-2 variants using a previously established protocol (**Extended data Fig. 1**).[12,13] The infectious cDNA clones enabled us to prepare recombinant Alpha and Delta SARS-CoV-2 variants (**Fig. 1a**). Both Alpha and Delta variants rescued from these clones developed smaller plaques on Vero E6 cells than the earlier USA/WA1-2020 (wild-type) strain isolated in January 2020 (**Extended data Fig. 2**). Sequencing analysis showed no undesired mutations in the rescued recombinant virus stocks. To compare the viral replication fitness between the Alpha and Delta variants, we performed a competition assay by infecting cells with a mixture of the two viruses at a plaque-forming unit (PFU) ratio of 1:1, followed by quantifying the ratios of the two viral RNA species at different days post infection. Compared with analyzing individual viruses separately, the competition assay has the advantages of (i) a built-in internal control of each viral replication and (ii) elimination of host-to-host variation that reduces experimental power. Due to its precision and reproducibility[14], the competition assay has been widely used to study microbial fitness,[15-17] including SARS-CoV-2[1,18]. When infecting human lung adenocarcinoma Calu-3 cells, the RNA ratio of Delta versus Alpha increased to 3.0, 7.0, and 4.1 at 24, 36, and 48 h post infection, respectively (**Extended data Fig. 3**). When infecting primary human airway epithelial (HAE) cultures, the RNA ratio of

Delta versus Alpha increased from 1.7 on day 1 to 3.1 on day 5 (**Fig. 1b**). These results indicate that Delta variant has greater replication fitness compared to the Alpha variant in *in vitro* respiratory models of SARS-CoV-2 infection.

To examine if the spike gene alone determines the improved replication fitness of the Delta variant, we constructed a chimeric Delta SARS-CoV-2 bearing the Alpha-spike glycoprotein (*i.e.*, Alpha-spike/Delta-backbone virus; **Fig. 1a** and **Extended data Fig. 2b**). In a competition assay on HAE culture, the RNA ratio of Delta versus Alpha-spike/Delta-backbone continuously increased from 2.8 on day 1 to 9.8 on day 5 post infection (**Fig. 1c**), suggesting that (i) the Alpha-spike reduces the replication fitness of the Delta variant and (ii) the spike gene drives the improved replication of Delta variant. Interestingly, the Alpha-spike/Delta-backbone virus replicated less efficiently than the Alpha variant on HAE culture (**Fig. 1d**), suggesting that, in contrast to Delta spike mutations that enhance replication, mutations outside the spike gene of the Delta variant reduced to some degree fitness for viral replication. The above quantifications of viral competition outcomes were measured by Sanger sequencing (**Fig. 1b-d**) and subsequently verified by Illumina next generation sequencing (NGS; **Extended data Fig. 4**).

Delta spike has accumulated mutations T19R, G142D, E156G, F157-R158 deletion, L452R, T478K, D614G, P681R, and D950N,[19] among which P681R is located at a furin cleavage site (PRRAR↓S with P681 underlined and "↓" indicating furin cleavage) that is absent in other group 2B coronaviruses.[20] Since the furin cleavage site was shown to be important for SARS-CoV-2 replication and pathogenesis,[21,22] we hypothesized that mutation P681R may improve the furin cleavage efficiency of full-length spike to S1 and S2, leading to a more efficient virus entry into respiratory epithelial cells. To test this hypothesis, we reverted the Delta P681R mutation to wild-type P681 in the Delta SARS-CoV-2 (**Extended data Fig. 2a**). The Delta-P681 virus developed equivalent plaque morphology compared with Delta (**Extended**

data Fig. 2b). Remarkably, the P681 reversion attenuated Delta variant replication on HAE cultures, as evidenced by the increase in the RNA ratio of wild-type Delta versus Delta-P681 from 2.2 on day 1 to 3.4 on day 5 (**Fig. 1e**). The replication of the Delta-P681 virus was even lower than that of the Alpha variant, as suggested by the decrease in the RNA ratio of Delta-P681 versus Alpha variant from 0.9 on day 1 to 0.6 on day 5 (**Fig. 1f**). These results demonstrate that mutation P681R at the furin cleavage site plays a critical role in enhancing the replication of the Delta variant on primary human airway cultures.

We directly evaluated the spike cleavage of Alpha, Delta, Delta-P681, and wild-type SARS-CoV-2. Virions were prepared from Vero E6 cells expressing TMPRSS2, a host serine protease that is required for SARS-CoV-2 entry via the ACE2-mediated cell surface mechanism.[23] After virions were purified through sucrose cushion ultracentrifugation, pelleted viruses were analyzed for spike cleavage by Western blotting (**Fig. 1g**). The results showed that spike processing efficiency of the purified virions occurred in the order of Delta > Alpha > Delta-P681 > wild-type virions, with ratios of S1 versus full-length spike of 15.3, 5.4, 2.7, and 1.4, respectively (**Fig. 1h**). It should be noted that the Alpha variant also has a spike mutation at amino acid position 681 (P681H), which may contribute to the increase in spike cleavage when compared with the wild-type USA/WA1-2020 virus; however, a recent study showed that mutation P681H alone did not enhance viral fitness or transmission.[4] Overall, our results indicate a correlation of improved spike cleavage with enhanced viral replication of Delta variant.

To exclude the possibility that enhanced replication of the Delta variant over Alpha was due to an improved spike/ACE2 receptor interaction, we performed a binding assay using recombinant spike receptor-binding domain (RBD) and human ACE2 proteins on a Bio-Layer Interferometry (BLI) system (**Extended data Fig. 5**). Within the RBD, the Alpha RBD has a N501Y mutation, whereas Delta RBD has L452R and T478K mutations. The BLI results indicate

that the Alpha RBD has a higher binding affinity for ACE2 than Delta RBD, as indicated by >200-fold K_D improvement (**Extended data Fig. 5**). These data strongly argue that the higher replication of Delta variant than Alpha variant is not due to an improved spike/ACE2 receptor binding.

Discussion

Since the emergence of SARS-CoV-2, the virus has accumulated mutations improving fitness and transmission. First, it accumulated a D614G mutation in the spike gene to enhance viral transmission.[1,3,6,24] This mutation promotes spike RBD in an "open" conformation to facilitate ACE2 receptor binding.[25] Subsequently, another spike mutation N501Y emerged independently in Alpha, Beta, and Gamma variants from the United Kingdom, South Africa, and Brazil, respectively. The N501Y mutation further increases the binding affinity between the spike protein and ACE2, leading to additional improvement in viral transmission.[4,10,26] Most recently, the Delta variant emerged and spread explosively, replacing the Alpha variant around the world. The current study demonstrates that spike mutation(s) are responsible for the enhanced viral fitness of the Delta variant over Alpha. Importantly, the unique P681R mutation plays a critical role in this fitness advantage and increases the processing of Delta spike to S1 and S2, most likely through an improved furin cleavage when newly assembled virions egress through the trans-Golgi network. Although the original SARS-CoV-2 strain has a functional furin cleavage site with a minimal recognition site of RXXR↓,[27] adjacent residues influence the cleavage efficiency.[28] The P681R substitution clearly augments spike processing and is likely the main driver of the fitness advantage observed in Delta variant. When the Delta variant infects respiratory epithelial cells, it binds to ACE2 receptor via the RBD in S1. Already cleaved at the S1/S2 site, the Delta virion facilitates cleavage at S2' by the cell surface protease TMPRSS2, leading to an activation of the S2 fusion peptide (FP) for viral and plasma membrane fusion.[23]

Thus, the improved spike cleavage enhances viral replication when the Delta variant infects respiratory epithelial cells.

One major concern with the emergence of Delta variant is its association with increased breakthrough infections in vaccinated people.[5,9] As a critical target for host immunity, changes in the spike protein of SARS-CoV-2 variants have been implicated in reducing antibody neutralization.[29] Among all tested variants (including Delta), the Beta and Kappa variants have been shown to reduce the BNT162b2 vaccine-elicited neutralizing titers the most;[2,30-32] yet, BNT162b2 showed 100% vaccine efficacy against Beta variant-associated severe, critical or fatal disease in Qatar and 100% real-world effectiveness against Beta variant-associated COVID-19 in South Africa.[33,34] These real-world vaccine efficacy/effectiveness and *in vitro* neutralization results argue that breakthrough infections by the Delta variant in vaccinated individuals do not reflect immune escape. Instead, the increased breakthrough infection is likely due to enhanced viral replication fitness of the Delta variant through augmented spike processing. Consistent with this hypothesis, the viral RNA loads in the oropharynx from Delta variant-infected patients were >1,200-fold higher than those from the original Wuhan virus-infected patients.[9] Together, the results indicate changes in viral processing and infection efficiency, rather than evasion of antibodies, drive breakthrough infections of Delta variant in vaccinated individuals.

In summary, using a reverse genetic system and primary human airway cultures, we have identified spike mutation P681R as a significant determinant for enhanced viral replication fitness of the Delta compared to the Alpha variant. The P681R mutation enhances spike protein processing through the improved furin cleavage site. As new variants continue to emerge, spike mutations that affect furin cleavage efficiency, as well as other mutations that may increase viral replication, pathogenesis, and/or immune escape, must be closely monitored.

Methods

Cells. African green monkey kidney epithelial Vero E6 cells (ATCC, Manassas, VA, USA) were grown in Dulbecco's modified Eagle's medium (DMEM; Gibco/Thermo Fisher, Waltham, MA, USA) with 10% fetal bovine serum (FBS; HyClone Laboratories, South Logan, UT) and 1% penicillin/streptomycin (Gibco). Human lung adenocarcinoma epithelial Calu-3 cells (ATCC) were maintained in a high-glucose DMEM containing sodium pyruvate and GlutaMAX (Gibco) with 10% FBS and 1% penicillin/streptomycin at 37°C with 5% CO_2. The EpiAirway system is a primary human airway 3D tissue model purchased from MatTek Life Science (Ashland, MA, USA). This EpiAirway system was maintained with the provided culture medium at 37°C with 5% CO_2 following manufacturer's instruction. All other culture medium and supplements were purchased from Thermo Fisher Scientific (Waltham, MA, USA). All cell lines were verified and tested negative for mycoplasma.

Construction of infectious cDNA clones and SARS-CoV-2 mutant viruses. The full-length (FL) cDNA clones of Alpha and Delta variants were constructed through mutagenesis of a previously established cDNA clone of USA/WA1-2020 SARS-CoV-2.[12,13] The previous seven-fragment *in vitro* ligation method was improved to a three-fragment ligation approach (**Extended data Fig. 1a**) to construct the full-length cDNA clones of Alpha and Delta SARS-CoV-2, resulting in Alpha-FL and Delta-FL, respectively. Prior to the three-fragment ligation, mutations from Alpha or Delta variants were engineered into individual fragments of USA/WA1-2020 using a standard mutagenesis method. The sequences for constructing Alpha, Delta and Alpha-spike/Delta-backbone were downloaded from GISAID database, the accession ID for Alpha is EPI_ISL_999340, accession ID for Delta is EPI_ISL_2100646. Individual point mutations for Alpha (NSP3: P153L, T183I, A890D, I1412T; NSP6: SGF106-108del; NSP12: P323L; Spike: HV69-70del, Y145del, N501Y, A570D, D614G, P681H, T716I, S982A, D1118H; ORF8: Q27stop, R52I, Y73C, S84L; N: D3L, R203K, G204R, S235F) and individual point mutations for

Delta (NSP2: P129L; NSP3: P822L; H1274Y; NSP4: A446V; NSP6: V149A; NSP12: P323L; V355A; G671S; NSP13: P77L; NSP15: H234Y; Spike: T19R, G142D, E156G, FR157-158del, L452R, T478K, D614G, P681R, D950N; ORF3a: S26L; M: I82T; ORF7a: V82A; L116F; T120I; ORF8: S84L; DF119-120del; N: D63G; R203M; D377Y; R385K) were introduced into subclones of individual fragments by overlapping fusion PCR. For preparing Alpha-spike/Delta-backbone virus, the spike gene of Delta was replaced with the spike gene of the Alpha. For preparing Delta-P681 virus, the P681 reversion was introduced into a subclone containing Delta spike gene by overlapping fusion PCR. All primers used for the construction were listed in **Extended Data Table 1**. The full-length infectious clones of SARS-CoV-2 variants were assembled by *in vitro* ligation of contiguous DNA fragments. *In vitro* transcription was then performed to synthesize full-length genomic RNA. For recovering recombinant viruses, the RNA transcripts were electroporated into Vero E6 cells. The viruses from electroporated cells were harvested at 40 h post electroporation and served as P0 stocks. All viruses were passaged once on Vero E6 cells to produce P1 stocks for subsequent experiments. All P1 viruses were subjected to next generation sequencing to confirm the introduced mutations without undesired changes. Viral titers were determined by plaque assay on Vero E6 cells. All virus preparation and experiments were performed in a biosafety level 3 (BSL-3) facility. Viruses and plasmids are available from the World Reference Center for Emerging Viruses and Arboviruses (WRCEVA) at the University of Texas Medical Branch.

RNA extraction, RT-PCR, and Sanger sequencing. Cell culture supernatants were mixed with a five-fold excess of TRIzol™ LS Reagent (Thermo Fisher Scientific, Waltham, MA, USA). Viral RNAs were extracted according to the manufacturer's instructions. The RNAs were amplified using a SuperScript™ III One-Step RT-PCR kit (Invitrogen, Carlsbad, CA, USA) following the manufacturer's protocol. The size of desired amplicon was verified with 2 µl of PCR product on an agarose gel. The remaining 18 µl of RT-PCR DNA was purified by a

QIAquick PCR Purification kit (Qiagen, Germantown, MD, USA). Sequences of the purified RT-PCR products were generated using a BigDye Terminator v3.1 cycle sequencing kit (Applied Biosystems, Austin, TX, USA). The sequencing reactions were purified using a 96-well plate format (EdgeBio, San Jose, CA, USA) and analyzed on a 3500 Genetic Analyzer (Applied Biosystems, Foster City, CA). The peak electropherogram height representing each mutation site and the proportion of each competitor was analyzed using the QSVanalyser program. For the competition assay, R software is used for the figure generation and statistical analysis. The presented viral RNA ratios in the figures were normalized by the input viral RNA ratios (**Extended Data Table 2**).

Plaque assay. Approximately 1.2×10^6 Vero E6 cells were seeded to each well of 6-well plates and cultured at 37°C, 5% CO_2 for 16 h. Virus was serially diluted in DMEM with 2% FBS and 200 µl diluted viruses were transferred onto the cell monolayers. The viruses were incubated with the cells at 37°C with 5% CO_2 for 1 h. After the incubation, overlay medium was added to the infected cells per well. The overlay medium contained DMEM with 2% FBS, 1% penicillin/streptomycin, and 1% sea-plaque agarose (Lonza, Walkersville, MD). After 2.5-day incubation, plates were stained with neutral red (Sigma-Aldrich, St. Louis, MO, USA) and plaques were counted on a light box.

Next generation sequencing (NGS). The competition results generated by Sanger sequencing were confirmed using NGS methods. Briefly, viral RNA samples from competition groups of (i) Delta versus Alpha and (ii) Delta versus Alpha-spike/Delta-backbone were used for a specific one-step RT-PCR that containing the A23063T mutation site. Viral RNA samples from competition group of Alpha versus Alpha-spike/Delta-backbone were quantified by the T14444C mutation. The RT-PCR primers were listed in **Extended Data Table 1**. The PCR products were purified by a QIAquick PCR Purification kit (Qiagen, Germantown, MD) according to the manufacturer's protocol. Dual-indexed adapter sequences (New England BioLabs, Ipswich, MA)

were added with 5 cycles of PCR. Samples were pooled and sequenced on an Illumina MiniSeq Mid-Output flow cell with the paired-end 150 base protocol. The reads were filtered for Q-scores of 37 at the A23063T and T14444C mutation sites and adjacent bases and counted. For the competition assay, R software is used for the figure generation and statistical analysis.

Viral infection of cell lines. Approximately 3×10^5 Calu-3 cells were seeded onto each well of 12-well plates and cultured at 37°C, 5% CO_2 for 16 h. Equal PFUs of two viruses were inoculated onto Calu-3 cells at a final MOI of 0.1. The mixed viruses were incubated with the cells at 37°C for 2 h. After infection, the cells were washed thrice with DPBS to remove residual viruses. One milliliter of culture medium was added into each well. At each time point, 100 µl of culture supernatants were lysed in TRIzol LS reagent for the detection of competition assay, and 100 µl of fresh medium was added into each well to replenish the culture volume. The cells were infected in triplicate for each group of viruses. All samples were stored at -80°C until analysis.

Primary human airway cultures. The EpiAirway system is a primary human airway 3D mucociliary tissue model consisting of normal, human-derived tracheal/bronchial epithelial cells. Different combinations of mixed viruses for competition assays were inoculated onto the culture at a total MOI of 5. After 2 h infection at 37 °C with 5% CO_2, the inoculum was removed, and the culture was washed three times with DPBS. The infected epithelial cells were maintained without any medium in the apical well, and medium was provided to the culture through the basal well. The infected cells were incubated at 37 °C, 5% CO_2. From day 1 to day 5 post infection, 300 µl of DPBS were added onto the apical side of the airway culture and incubated at 37°C for 30 min to elute progeny viruses. All virus samples in DPBS were stored at −80°C and quantified by plaque assays on Vero E6 cells.

Virion purification and Western blotting. Vero E6 expressing TMPRSS2 were infected with different SARS-CoV-2 at an MOI of 0.01. At 24 h post infection, the culture

medium was collected, purified through a 20% sucrose cushion, and analyzed by Western blot as previously described.[21] Densitometry was performed to quantify the cleavage efficiency of full-length spike to S1/S2 subunits using ImageLab 6.0.1 (Bio-Rad #12012931). The average results of two experiments were presented.

Spike RBD and ACE2 binding. The human ACE2 protein was purchased from Sino Biological (Beijing, China; Cat# 10108-H08H) and the human IgG1 Fc-tagged RBD proteins were made in-house using a method as previously described[35]. The affinity measurement was performed on the ForteBio Octet RED 96 system (Sartorius, Goettingen, Germany). Briefly, the RBD proteins (20 µg/ml) of Alpha or Delta RBDs were captured onto protein A biosensors for 300s. The loaded biosensors were then dipped into the kinetics buffer for 10 s for adjustment of baselines. Subsequently, the biosensors were dipped into serially diluted (from 1.23 to 300 nM) human ACE2 protein for 200 s to record association kinetics and then dipped into kinetics buffer for 400 s to record dissociation kinetics. Kinetic buffer without ACE2 was used to correct the background. The Octet Data Acquisition 9.0 software was used to collect affinity data. For fitting of K_D values, Octet Data Analysis software V11.1 was used to fit the curve by a 1:1 binding model using the global fitting method.

Statistics. For virus competition experiments, relative replicative fitness values for different variants were analyzed according to w=(f0/i0), where i0 is the initial two-virus ratio and f0 is the final two-virus ratio after competition. Sanger sequencing (initial timepoint T0) counts for each virus being compared were based upon average counts over three replicate samples of inocula per experiment, and post-infection (timepoint T1) counts were taken from samples of individual subjects. Multiple experiments were performed, so that f0/i0 was clustered by experiment. To model f0/i0, the ratio T0/T1 was found separately for each subject in each virus group, log (base-10) transformed to an improved approximation of normality and modeled by analysis of variance with relation to group, adjusting by experiment when appropriate to control

for clustering within experiment. Specifically, the model was of the form Log10_CountT1overCountT0 ~ Experiment + Group. Fitness ratios between the two groups [the model's estimate of w=(f0/i0)] were assessed per the coefficient of the model's Group term, which was transformed to the original scale as 10^coefficient. This modeling approach compensates for any correlation due to clustering within experiment similarly to that of corresponding mixed effect models and is effective since the number of experiments was small. Statistical analyses were performed using R statistical software (R Core Team, 2019, version 3.6.1). In all statistical tests, two-sided alpha=.05. Catseye plots[36], which illustrate the normal distribution of the model-adjusted means, were produced using the "catseyes" package[37].

Data availability.

Extended Data and source data for generating main figures are available in the online version of the paper. Any other information is available upon request.

Acknowledgments

P.-Y.S. was supported by National Institutes of Health (NIH) grants AI134907 and UL1TR001439, and awards from the Sealy and Smith Foundation, the Kleberg Foundation, the John S. Dunn Foundation, the Amon G. Carter Foundation, the Gillson Longenbaugh Foundation, and the Summerfield Robert Foundation. Z.A. was supported in by a Welch Foundation grant AU-0042-20030616 and Cancer Prevention and Research Institute of Texas (CPRIT) Grants RP150551 and RP190561. S.C.W. was supported by NIH grant R24 AI120942. V.D.M. was supported by NIH grants AI153602 and 1R21AI145400. J.L. and B.A.J. were supported by James W. McLaughlin Fellowship Fund.

Author contributions

Conceptualization, Y.L., J.L., S.C.W., V.D.M., X.X., P.-Y.S.; Methodology, Y.L., J.L., B.A.J., H.X., Z.K., C.S., S.G.W., Z.A., X.X.; Investigation, Y.L., J.L., B.A.J., H.X., Z.A., S.C.W., V.D.M., X.X., P.-Y.S.; Resources, H.X., B.A.J., Z.K., Z.A. X.X.; Data Curation, Y.L., J.L., B.A.J., H.X., Z.K., C.S., S.C.W., V.D.M., X.X., P.-Y.S.; Writing-Original Draft, Y.L., J.L, X.X., P.-Y.S; Writing-Review & Editing, Y.L., J.L., B.A.J., H.X., Z.K., C.S., S.G.W., Z.A., S.C.W., V.D.M., X.X., P.-Y.S.; Supervision, X.X., S.C.W., V.D.M., P.-Y.S.; Funding Acquisition, Z.A., S.C.W., V.D.M., P.-Y.S.

Competing financial interests

X.X., V.D.M., and P.-Y.S. have filed a patent on the reverse genetic system and reporter SARS-CoV-2. Other authors declare no competing interests.

References

1 Plante, J. A. *et al.* Spike mutation D614G alters SARS-CoV-2 fitness. *Nature* **592**, 116-121, doi:10.1038/s41586-020-2895-3 (2021).

2 Chen, R. E. *et al.* Resistance of SARS-CoV-2 variants to neutralization by monoclonal and serum-derived polyclonal antibodies. *Nat Med* **27**, 717-726, doi:10.1038/s41591-021-01294-w (2021).

3 Hou, Y. J. *et al.* SARS-CoV-2 D614G variant exhibits efficient replication ex vivo and transmission in vivo. *Science* **370**, 1464-1468, doi:10.1126/science.abe8499 (2020).

4 Liu, Y. *et al.* The N501Y spike substitution enhances SARS-CoV-2 transmission. *bioRxiv*, doi:10.1101/2021.03.08.434499 (2021).

5 Brown, C. M. *et al.* Outbreak of SARS-CoV-2 Infections, Including COVID-19 Vaccine Breakthrough Infections, Associated with Large Public Gatherings — Barnstable County, Massachusetts, July 2021. *Morbidity and Mortality Weekly Report (MMWR)*, https://www.cdc.gov/mmwr/volumes/70/wr/mm7031e7032.htm?s_cid=mm7031e7032_w&fbclid=IwAR7032WV7036ul_A-l_VN_7015KX7034bedb7038CeLJKRwiDWZ-blUuWmZMKbs7094xdhTiPLs (2021).

6 Zhou, B. *et al.* SARS-CoV-2 spike D614G change enhances replication and transmission. *Nature* **592**, 122-127, doi:10.1038/s41586-021-03361-1 (2021).

7 WHO. Track SARS-CoV-2 variants. https://www.who.int/en/activities/tracking-SARS-CoV-2-variants/ (2021).

8 CDC. COVID data tracker. https://covid.cdc.gov/covid-data-tracker/#variant-proportions (2021).

9 Li, B. *et al.* Viral infection and transmission in a large, well-traced outbreak caused by the SARS-CoV-2 Delta variant. *medRxiv*, https://www.medrxiv.org/content/10.1101/2021.1107.1107.21260122v21260122 (2021).

10 MIcochova, P. *et al.* SARS-CoV-2 B.1.617.2 Delta variant emergence, replication and sensitivity to neutralising antibodies. *BioRxiv* (2021).

11 Chia, P. Y. *et al.* Virological and serological kinetics of SARS-CoV-2 Delta variant vaccine2 breakthrough infections: a multi-center cohort study. *medRxiv*, https://www.medrxiv.org/content/10.1101/2021.1107.1128.21261295v21261291 (2021).

12 Xie, X. *et al.* An Infectious cDNA Clone of SARS-CoV-2. *Cell Host Microbe* **27**, 841-848 e843, doi:10.1016/j.chom.2020.04.004 (2020).

13 Xie, X. *et al.* Engineering SARS-CoV-2 using a reverse genetic system. *Nature Protocols* **16**, 1761-1784, doi:10.1038/s41596-021-00491-8 (2021).

14 Liu, J. *et al.* Role of mutational reversions and fitness restoration in Zika virus spread to the Americas. *Nat Commun* **12**, 595, doi:10.1038/s41467-020-20747-3 (2021).

15 Wiser, M. J. & Lenski, R. E. A Comparison of Methods to Measure Fitness in Escherichia coli. *PLoS One* **10**, e0126210, doi:10.1371/journal.pone.0126210 (2015).

16 Grubaugh, N. D. *et al.* Genetic Drift during Systemic Arbovirus Infection of Mosquito Vectors Leads to Decreased Relative Fitness during Host Switching. *Cell Host Microbe* **19**, 481-492, doi:10.1016/j.chom.2016.03.002 (2016).

17 Bergren, N. A. *et al.* "Submergence" of Western equine encephalitis virus: Evidence of positive selection argues against genetic drift and fitness reductions. *PLoS Pathog* **16**, e1008102, doi:10.1371/journal.ppat.1008102 (2020).

18 Touret, F. *et al.* Replicative Fitness of a SARS-CoV-2 20I/501Y.V1 Variant from Lineage B.1.1.7 in Human Reconstituted Bronchial Epithelium. *mBio*, e0085021, doi:10.1128/mBio.00850-21 (2021).

19 Organization, W. H. Coronavirus Disease (COVID-19): Weekly Epidemiological Update. *https://reliefweb.int/report/world/coronavirus-disease-covid-19-weekly-epidemiological-update-11-may-2021* (2021).

20 Coutard, B. *et al.* The spike glycoprotein of the new coronavirus 2019-nCoV contains a furin-like cleavage site absent in CoV of the same clade. *Antiviral Res* **176**, 104742, doi:10.1016/j.antiviral.2020.104742 (2020).

21 Johnson, B. A. *et al.* Loss of furin cleavage site attenuates SARS-CoV-2 pathogenesis. *Nature* **591**, 293-299, doi:10.1038/s41586-021-03237-4 (2021).

22 Peacock, T. P. *et al.* The furin cleavage site in the SARS-CoV-2 spike protein is required for transmission in ferrets. *Nat Microbiol* **6**, 899-909, doi:10.1038/s41564-021-00908-w (2021).

23 Murgolo, N. *et al.* SARS-CoV-2 tropism, entry, replication, and propagation: Considerations for drug discovery and development. *PLoS Pathog* **17**, e1009225, doi:10.1371/journal.ppat.1009225 (2021).

24 Korber, B. *et al.* Tracking Changes in SARS-CoV-2 Spike: Evidence that D614G Increases Infectivity of the COVID-19 Virus. *Cell* **182**, 812-827 e819, doi:10.1016/j.cell.2020.06.043 (2020).

25 Yurkovetskiy, L. *et al.* Structural and Functional Analysis of the D614G SARS-CoV-2 Spike Protein Variant. *Cell* **183**, 739-751, doi:10.1016/j.cell.2020.09.032 (2020).

405 26 Wan, Y., Shang, J., Graham, R., Baric, R. S. & Li, F. Receptor Recognition by the Novel Coronavirus
406 from Wuhan: an Analysis Based on Decade-Long Structural Studies of SARS Coronavirus. *J Virol*
407 **94**, doi:10.1128/JVI.00127-20 (2020).
408 27 Molloy, S. S., Bresnahan, P. A., Leppla, S. H., Klimpel, K. R. & Thomas, G. Human furin is a
409 calcium-dependent serine endoprotease that recognizes the sequence Arg-X-X-Arg and
410 efficiently cleaves anthrax toxin protective antigen. *Journal of Biological Chemistry* **267**, 16396-
411 16402 (1992).
412 28 Krysan, D. J., Rockwell, N. C. & Fuller, R. S. Quantitative characterization of furin specificity.
413 Energetics of substrate discrimination using an internally consistent set of hexapeptidyl
414 methylcoumarinamides. *J Biol Chem* **274**, 23229-23234, doi:10.1074/jbc.274.33.23229 (1999).
415 29 Plante, J. A. *et al.* The variant gambit: COVID-19's next move. *Cell Host Microbe* **29**, 508-515,
416 doi:10.1016/j.chom.2021.02.020 (2021).
417 30 Liu, Y. *et al.* Neutralizing Activity of BNT162b2-Elicited Serum. *N Engl J Med* **384**, 1466-1468,
418 doi:10.1056/NEJMc2102017 (2021).
419 31 Liu, Y. *et al.* BNT162b2-Elicited Neutralization against New SARS-CoV-2 Spike Variants. *N Engl J*
420 *Med*, doi:10.1056/NEJMc2106083 (2021).
421 32 Liu, J. *et al.* BNT162b2-elicited neutralization of B.1.617 and other SARS-CoV-2 variants. *Nature*,
422 doi:10.1038/s41586-021-03693-y (2021).
423 33 Abu-Raddad, L. J., Chemaitelly, H., Butt, A. A. & National Study Group for, C.-V. Effectiveness of
424 the BNT162b2 Covid-19 Vaccine against the B.1.1.7 and B.1.351 Variants. *N Engl J Med* **385**, 187-
425 189, doi:10.1056/NEJMc2104974 (2021).
426 34 Thomas, S. J. *et al.* Six Month Safety and Efficacy of the BNT162b2 mRNA COVID-19 Vaccine. *N*
427 *Engl J Med* In press (2021).
428 35 Ku, Z. *et al.* Molecular determinants and mechanism for antibody cocktail preventing SARS-CoV-
429 2 escape. *Nat Commun* **12**, 469, doi:10.1038/s41467-020-20789-7 (2021).
430 36 Cumming, G. The New Statistics: Why and How. *Psychol. Sci.*, 7-29,
431 doi:10.1177/0956797613504966 (2014).
432 37 Andersen, C. Catseyes: Create Catseye Plots Illustrating the Normal Distribution of the Means. R
433 package version 0.2.3. (2019).

434

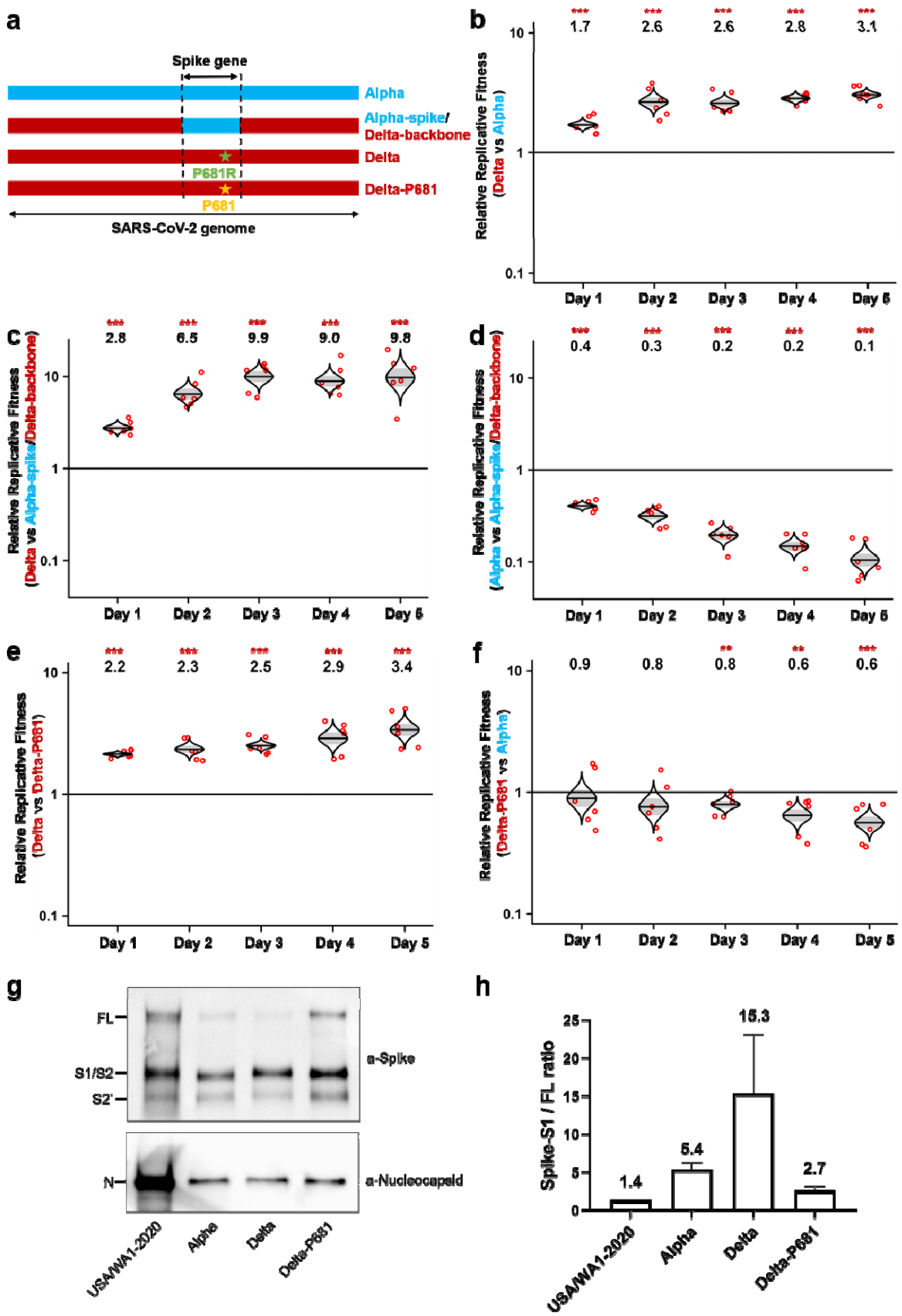
a
Spike gene
Alpha
Alpha-spike/
Delta-backbone
Delta
P681R
Delta-P681
P681
SARS-CoV-2 genome
b
Relative Replicative Fitness
(Delta vs Alpha)
1.7
2.6
2.6
2.8
3.1
Day 1
Day 2
Day 3
Day 4
Day 5
c
Relative Replicative Fitness
(Delta vs Alpha-spike/Delta-backbone)
2.8
6.5
9.9
9.0
9.8
d
Relative Replicative Fitness
(Alpha vs Alpha-spike/Delta-backbone)
0.4
0.3
0.2
0.2
0.1
e
Relative Replicative Fitness
(Delta vs Delta-P681)
2.2
2.3
2.5
2.9
3.4
f
Relative Replicative Fitness
(Delta-P681 vs Alpha)
0.9
0.8
0.8
0.6
0.6
g
FL
S1/S2
S2'
α-Spike
N
α-Nucleocapsid
USA/WA1-2020
Alpha
Delta
Delta-P681
h
Spike-S1 / FL ratio
1.4
5.4
15.3
2.7
USA/WA1-2020
Alpha
Delta
Delta-P681

435

Figure 1. Delta P681R mutation enhances SARS-CoV-2 fitness over Alpha variant through improving spike protein processing.

a, Schemes of Alpha variant, Delta variant, Delta variant bearing Alpha-spike, and Delta variant with a P681R-to-P681 reversion. The spike gene of Delta variant was swapped with Alpha variant, resulting in chimeric SARS-CoV-2 "Alpha-spike/Delta-backbone." The Delta P681R mutation was reverted wild-type P681, resulting in "Delta-P681" virus. Blue and red colors indicate Alpha and Delta variants, respectively. **b-f,** Viral replication competitions among Alpha, Delta, Alpha-spike/Delta-backbone, and Delta-P681 viruses on primary human airway epithelial (HAE) cells. Equal PFU of two viruses were mixed and inoculated onto HAE cells at an MOI of 5. Five pairs of viral competition are presented: Delta and Alpha (**b**), Delta and Alpha-spike/Delta-backbone (**c**), Alpha and Alpha-spike/Delta-backbone (**d**), Delta variant and Delta-P618 (**e**), and Delta-P681 and Alpha (**f**). After 2 h incubation, the cells were washed thrice with DPBS and maintained for 5 days. The secreted viruses were collected daily in DPBS after incubation at 37˚C for 30 min. Red dots represent individual cell cultures (n=6), the horizontal lines in each catseye represent the mean, shaded regions represent standard error of the mean; y-axes use a $\log_{10}$ scale. Black numbers above each set of values (catseye) indicate the ratios of two viral RNA species. *P* values are calculated for group coefficient using linear regression model. $^{**}p<0.01$, $^{***}p<0.001$. **g,** Spike cleavages of purified virions. USA/WA1-2020, Alpha, Delta, and Delta-P681 viruses were purified and analyzed by Western blot using polyclonal antibodies against spike and anti-nucleocapsid antibodies. Full-length spike (FL), cleaved S1/S2, and S2' proteins were annotated. One representative image of two experiments is shown. **h,** Quantification of spike processing of different variants from **g**. Densitometry was performed to quantify the cleavage efficiency of FL spike to S1/S2 subunits using ImageLab 6.0.1. The ratios of S1/S2 over FL were calculated to indicate spike processing efficiencies. The average results of two experiments were presented as mean ± standard deviation.

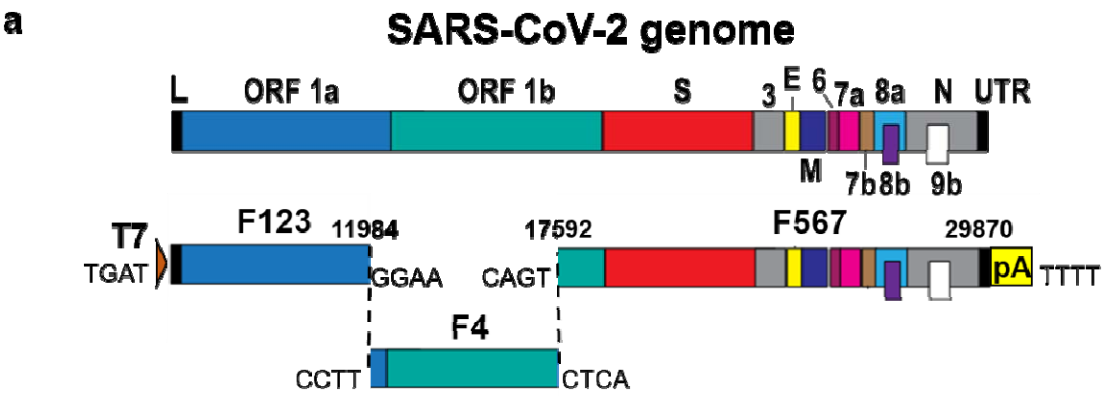

b Alpha

Gene	Nucleotide	Amino acid
5'UTR	C241T	
ORF1ab	C913T	
	C3037T	
	C3177T	P971L
	C3267T	T1001I
	C5388A	A1708D
	C5986T	
	T6954C	I2230T
	T8782C	
	11288-11296 deletion	SGF 3675-3677 deletion
	C14408T	P4715L
	C14676T	
	C15279T	
	T16176C	
Spike	21766-21771 deletion	HV 69-70 deletion
	21991-21993 deletion	Y144 deletion
	A23063T	N501Y
	C23271A	A570D
	A23403G	D614G
	C23604A	P681H
	C23709T	T716I
	T24506G	S982A
	G24914C	D1118H
ORF8	C27972T	Q27stop
	G28048T	R52I
	A28111G	Y73C
	C28144T	S84L
N	28280 GAT->CTA	D3L
	28881 GGG->AAC	R203K/G204R
	C28977T	S235F

c Delta

Gene	Nucleotide	Amino acid
5'UTR	C210T	
	C241T	
ORF1ab	C1191T	P309L
	C1267T	
	C3037T	
	C5184T	P1640L
	C6539T	H2092Y
	T8782C	
	C9891T	A3209V
	T11418C	V3718A
	T12946C	
	C14408T	P4715L
	T14444C	V4727A
	G15451A	G5063S
	C16466T	P5401L
	A20262G	
	C20320T	H6686Y
Spike	C21618G	T19R
	G21987A	G142D
	22029-22034 deletion	E156G/FR157-158 deletion
	T22917G	L452R
	C22995A	T478K
	A23403G	D614G
	C23604G	P681R
	G24410A	D950N
	C24745T	
ORF3a	C25469T	S26L
M	T26767C	M: I82T
ORF7a	T27638C	V82A
	C27739T	L116F
	C27752T	T120I
ORF8	C28144T	S84L
	28248-28253 deletion	DF119-120 deletion
N	A28461G	D63G
	G28881T	R203M
	G29402T	D377Y
	G29427A	R385K
3'UTR	G29742T	
	C29762T	

Extended Data Figure 1. Construction of infectious cDNA clones for Alpha and Delta variants.

a, Construction of infectious cDNA clones for Alpha and Delta variants. A three-fragment *in vitro* ligation was performed to construct the full-length cDNA clones of Alpha and Delta SARS-CoV-2.

The construction method was detailed previously.[12,13] ORFs, the Open reading frames; L, leader sequence; S, spike gene; E, envelope glycoprotein gene; M, membrane glycoprotein gene; N, nucleocapsid gene; UTR, untranslated region. **b,c,** Mutations from Alpha and Delta variants. The whole genome sequences of Alpha (EPI_ISL_999340) (**b**) and Delta (EPI_ISL_2100646) (**c**) were compared to USA/WA1-2020 strain. Nucleotide and amino acid mutations are presented.

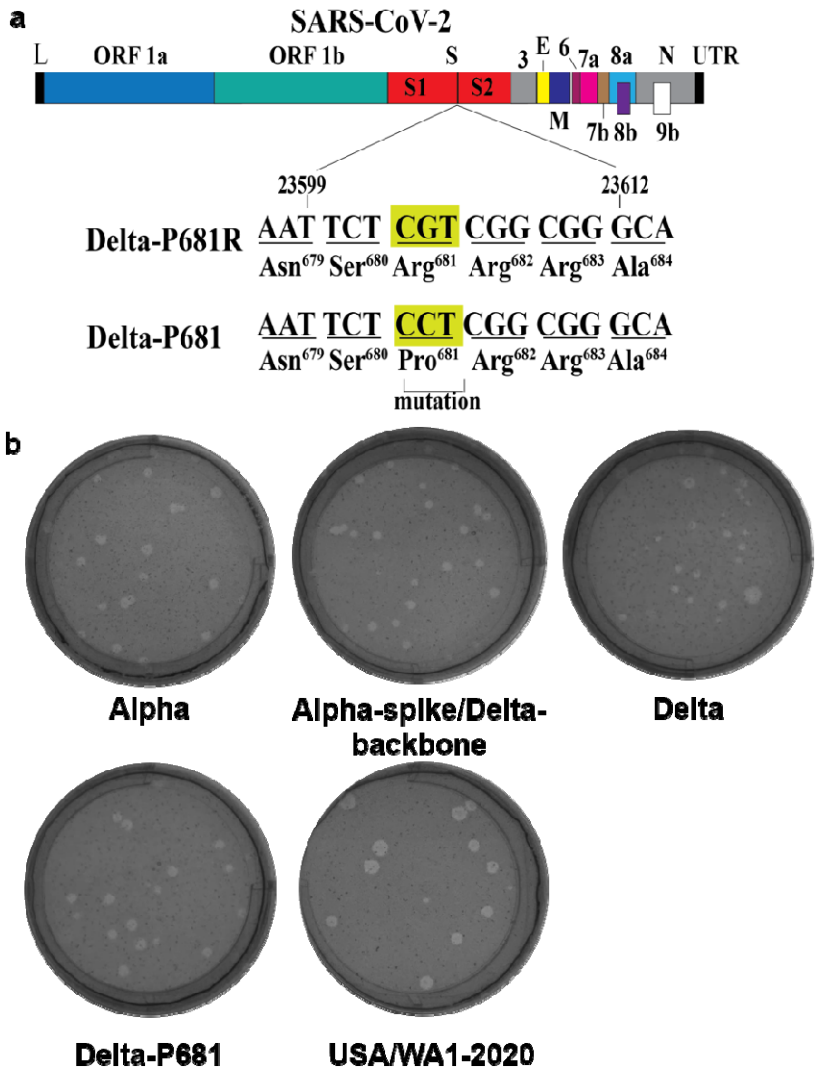

Extended Data Figure 2. Construction of Delta-P681 SARS-CoV-2 and plaque morphologies of different recombinant SARS-CoV-2s.
a, Construction of revertant Delta-P681 SARS-CoV-2. Single nucleotide G-to-C substitution was engineered into the Delta variant to construct Delta-P681 SARS-CoV-2. The nucleotide positions of viral genome are annotated. **b,** Plaque morphologies of Alpha, Alpha-spike/Delta-backbone, Delta, Delta-P681, and USA-WA1/2020 viruses. The plaque images were taken on day 2.5 post infection of Vero E6 cells.

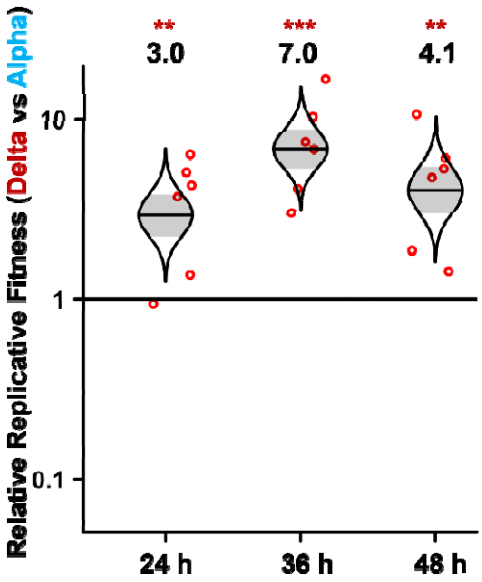

Extended Data Figure 3. Viral replication competition between Delta and Alpha variants on Calu-3 cells.
Recombinant Delta and Alpha SARS-CoV-2s were mixed in equal PFUs to infect Calu-3 cells at a total MOI of 0.1. At 2 h post infection, the cells were washed thrice with DPBS to remove free viruses. Culture medium were sampled for Sanger sequencing at 24 h, 36 h, and 48 h post infection. Red dots represent individual cell cultures (n=6); horizontal lines in each catseye represent the mean; shaded regions represent standard error of the mean; y-axes use a $\log_{10}$ scale. Black numbers above each set of values (catseye) indicate the ratios of two viral RNA species. *P* values are calculated for group coefficient using linear regression model. ***p*<0.01, ****p*<0.001.

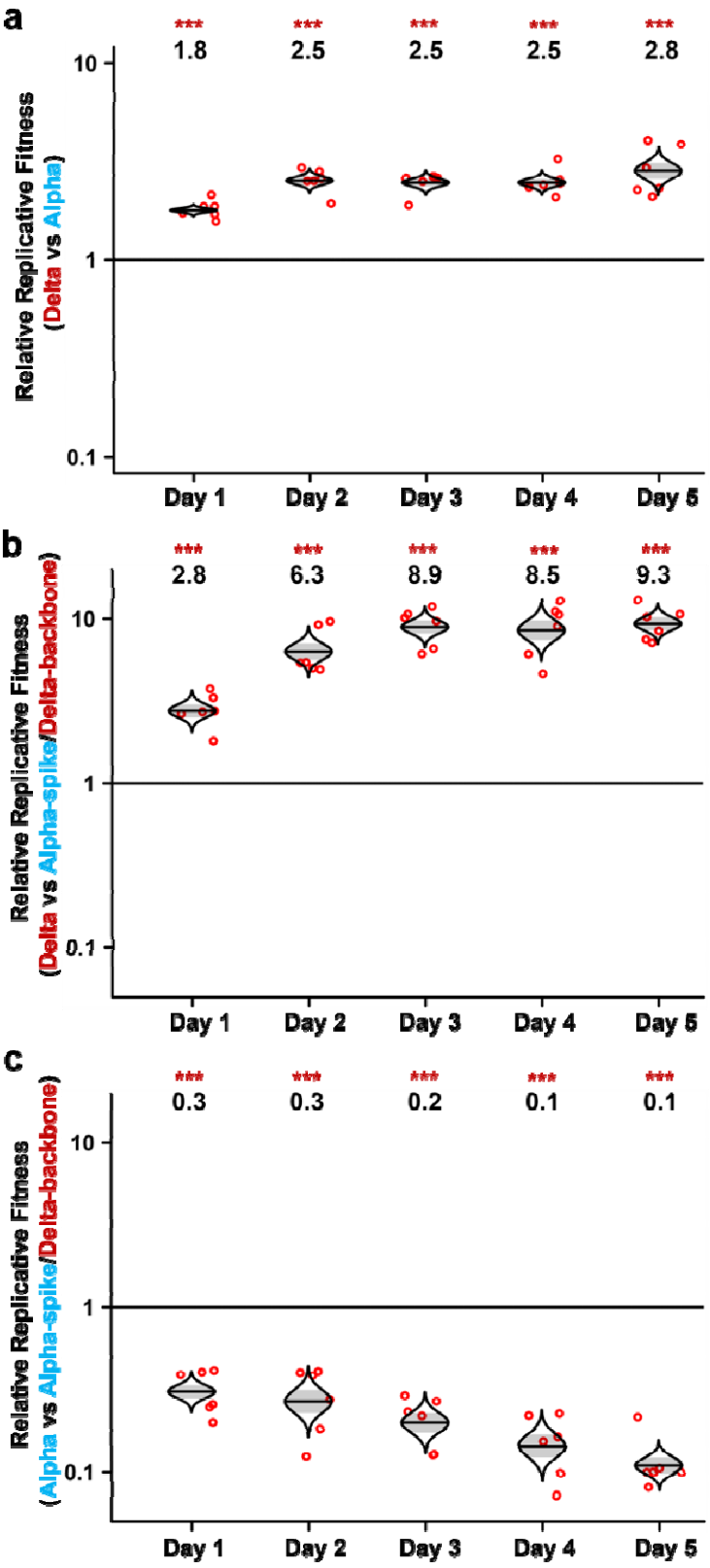
a
***
1.8
2.5
2.5
2.5
2.8
10
1
0.1
Relative Replicative Fitness
(Delta vs Alpha)
Day 1
Day 2
Day 3
Day 4
Day 5
b
***
2.8
6.3
8.9
8.5
9.3
10
1
0.1
Relative Replicative Fitness
(Delta vs Alpha-spike/Delta-backbone)
Day 1
Day 2
Day 3
Day 4
Day 5
c
***
0.3
0.3
0.2
0.1
0.1
10
1
0.1
Relative Replicative Fitness
(Alpha vs Alpha-spike/Delta-backbone)
Day 1
Day 2
Day 3
Day 4
Day 5

491

Extended Data Figure 4. Validation of viral competition results by next generation sequencing.

a-c, RNA samples from competition assays between Delta and Alpha (**a**), Delta and Alpha-spike/Delta-backbone (**b**), and Alpha and Alpha-spike/Delta-backbone (**c**) were initially assessed using Sanger sequencing (**Fig. 1b-d**). The same RNA samples were retested here using next generation sequencing (NGS). Red dots represent individual cell cultures (n=6); the horizontal lines in each catseye represent the mean; shaded regions represent standard error of the mean; y-axes use a $\log_{10}$ scale. Black numbers above each set of values (catseye) indicate the relative fitness estimates. *P* values are calculated for group coefficient using linear regression model. ***$p<0.001$.

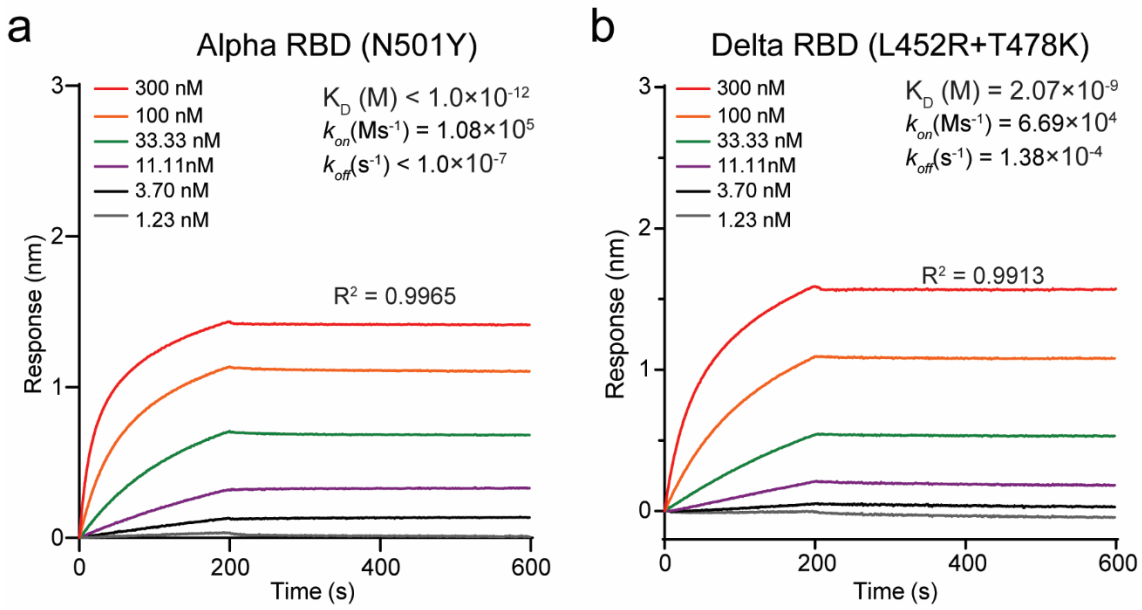

Extended Data Figure 5. Binding affinities of Alpha and Delta RBDs to human ACE2 receptor.

a-b, Alpha RBD (**a**) and Delta RBD (**b**) proteins were captured onto protein A biosensors. The biosensors were then dipped into serially diluted human ACE2 protein and buffers to measure the association and dissociation kinetics. The binding affinity-related parameters, including association (K_{on}), dissociation (K_{off}), and affinity (K_D) are shown. The affinity of ACE2 to Alpha RBD (N501Y) is below the detection limit and is presented as $<1.0\times10^{-12}$. The result for Alpha RBD and ACE2 binding was adopted from our previous study[4] for comparison.

Extended Data Table 1. Primer list used for SARS-CoV-2 infectious clones construction, RT-PCR and sequencing.

Construction of Alpha full length and Alpha-backbone infectious clone	Forward primer	Reverse primer
C241T	atctaggtttTgtccgggtgtgaccgaaag	ctttcggtcacacccggacAaaacctagat
C913T	tgcactttgtcTgaacaactggactt	aagtccagttgttcAgacaaagtgca
C3037T	gtattgttctttTtaccctccagatgagg	cctcatctggagggtaAaaagaacaatac
C3177T	ctgctcttcaacTtgaagaagagcaa	ttgctcttcttcaAgttgaagagcag
C3267T	cagacaactaTtattcaaacaattgttgagg	cctcaacaattgtttgaataAtagttgtctg
C5388A	ggctggtgaagctgAtaacttttgtgc	gcacaaaagttaTcagcttcaccagcc
C5986T	attcttatttTacagagcaaccaattg	caattggttgctctgtAaaataagaat
T6954C	gataaatattaCaatttggtttttac	gtaaaaaccaaattGtaatatttatc
11288-11296del	gatactagtttgaagctaaaagactgtgt	acacagtcttttagcttcaaactagtatc
C14408T	tacagtgttcccacTtacaagttttggacc	ggtccaaaacttgtaAgtgggaacactgta
C14676T	gtcaaaccTggtaattttaacaaag	ctttgttaaaattaccAggtttgac
C15279T	gaaaaccctcaTcttatgggttgggat	atcccaacccataagAtgagggttttc
T16176C	ctaatgataacacCtcaaggtattggga	tcccaataccttgaGgtgttatcattag
C27972T/G28048T	cttaacatcaaccatatgtagttgatgacccgtgtcctattcacttcta	ttatagctcctactctaatataccatttagaatagaagtgaataggaca
A28111G/C28144T	cagtgcatcgatatcggtaattatacagtttcctgtttacctttac	gtaaaaggtaaacaggaaactgtataattaccgatatcgatgcactg
A28271del/28280-28282GAT-CTA	caaactaaatgtctctaaatggaccccaaaatcagcg	cgctgattttggggtccatttagagacatttagtttg
28881-28883GGG-AAC	caactccaggcagcagtaaacgaacttctcctgc	gcaggagaagttcgtttactgctgcctggagttg
C28977T	tgagagcaaaatgtttggtaaaggccaaca	tgttggcctttaccaaacattttgctctca
Alpha-F123-F1	cattatacgaagttatattcgatgcggccgctaatacgactcactatagattaaag	gggccgacaacatgaagacagtg
Alpha-F123-F2	acactgtcttcatgttgtcggcccaaatgttaacaaag	ctattacgtttgtaacacatcatacaTgtAgatgaattac
Alpha-F123-F3	gtatgatgtgttacaaacgtaatagagcaacaagag	aggtcgactctagaggatcccacATCGAtggtctcaaaggcttcagtagtatctttagc
Alpha-F4	tgtagaaaacccagatatatt	caaaacactctacacgagcac
Alpha-F567-F1	tatacgaagttatattcgatgcggccgcgtctcagagtgcttttggtttatgataataag	cttttgttgtataaacccacaaatg
Alpha-F567-F2	catttgtgggtttatacaacaaaag	caatcaagccagctataaaacc
Alpha-F567-F3	ggttttatagctggcttgattg	cgaggcttcttagaagcctca
Alpha-backbone-F567-F1	tatacgaagttatattcgatgcggccgcgtctcagagtgcttttggtttatgataataag	cttttgttgtataaacccacaaatg
Alpha-backbone-F567-F2	catttgtgggtttatacaacaaaag	caatcaagccagctataaaacc
Alpha-backbone-F567-F3	ggttttatagctggcttgattg	cgaggcttcttagaagcctca

Construction of Delta full length and Delta-backbone infectious clone	Forward primer	Reverse primer
C210T	GTTTCGTCCGTTTTGCAGCCGATCATC	GATGATCGGCTGCAAAACGGACGAAAC
C241T	ATCTAGGTTTTGTCCGGGTGTGACCGAAAG	CTTTCGGTCACACCCGGACAAAACCTAGAT
C1191T	CCAGTTGCGTCACTAAATGAATGCAACC	GGTTGCATTCATTTAGTGACGCAACTGG
C1267T	GGCAGACGGGTGATTTTGTTAAAGCC	GGCTTTAACAAAATCACCCGTCTGCC
C3037T	GTATTGTTCTTTTTACCCTCCAGATGAGG	CCTCATCTGGAGGGTAAAAAGAACAATAC
C5184T	ACACAACTGATCTTAGTTTTCTGGGTAG	CTACCCAGAAAACTAAGATCAGTTGTGT
C6539T	GAGGTTGGCTACACAGATCTAATGGC	GCCATTAGATCTGTGTAGCCAACCTC
T8782C	ACACATGGTTTAGCCAGCGTGGTGGTAG	CTACCACCACGCTGGCTAAACCATGTGT
C9891T	GATACTTAGTTCTTTATAATAAGTACAAG	CTTGTACTTATTATAAAGAACTAAGTATC
T11418C	CTTGACACTCGCTTATAAAGTTTATTATGG	CCATAATAAACTTTATAAGCGAGTGTCAAG
T12946C	GGTCCTAAAGTGAAGTACTTATACTTTATT	AATAAAGTATAAGTACTTCACTTTAGGACC
C14408T	TACAGTGTTCCCACTTACAAGTTTTGGACC	GGTCCAAAACTTGTAAGTGGGAACACTGTA
T14444C	GTGAGAAAAATATTTGCTGATGGTGTTCCA	TGGAACACCATCAGCAAATATTTTTCTCAC
G15451A	GGTCATGTGTGGCAGTTCACTATATGTT	AACATATAGTGAACTGCCACACATGACC
C16466T	GTAAATCACATAAACTACCCATTAGTTTTCC	GGAAAACTAATGGGTAGTTTATGTGATTTAC
A20262G	GGAAATTGATTTCTTGGAATTAGCTATGG	CCATAGCTAATTCCAAGAAATCAATTTCC
C20320T	GCTATGCCTTCGAATATATCGTTTATGG	CCATAAACGATATATTCGAAGGCATAGC
C21618G	GTGTGTTAATCTTAGAACCAGAACTC	GAGTTCTGGTTCTAAGATTAACACAC
G21987A	GATCCATTTTTGGATGTTTATTACCAC	GTGGTAATAAACATCCAAAAATGGATC
22029-22034 deletion	GAAAGTGGAGTTTATTCTAGTGCGAATAATTGC	ATAAACTCCACTTTCCATCCAACTTTTGTTGTT
T22917G	GGTGGTAATTATAATTACCGGTATAGATTGTTTAGG	CCTAAACAATCTATACCGGTAATTATAATTACCACC
C22995A	GGCCGGTAGCAAACCTTGTAATGGTG	CACCATTACAAGGTTTGCTACCGGCC
A23604G	GACTAATTCTCGTCGGCGGGCACGTAGTGT	ACACTACGTGCCCGCCGACGAGAATTAGTC
G24410A	GGAAAACTTCAAAATGTGGTCAACC	GGTTGACCACATTTTGAAGTTTTCC
C24745T	CTCATGGTGTAGTTTTCTTGCATGTGAC	GTCACATGCAAGAAAACTACACCATGAG
C25469T	GATGCTACTCCTTTAGATTTTGTTCGCG	CGCGAACAAAATCTAAAGGAGTAGCATC
T26767C	CCGGTGGAATTGCTACCGCAATGGCTTG	CAAGCCATTGCGGTAGCAATTCCACCGG
T27638C	CGTGCCAGATCAGCTTCACCTAAACTGT	ACAGTTTAGGTGAAGCTGATCTGGCACG
C27739T/C27752T	TCAAAAGAAAGATAGAATGATTGAACTTTCA	CATTCTATCTTTCTTTTGAATGTGAAGCAAAGTG
C28144T	TCGGTAATTATACAGTTTCCTGTTTACCTTTTAC	GTAAAAGGTAAACAGGAAACTGTATAATTACCGA

28248-28253 deletion	GACGTTCGTGTTGTTTTAATCTAAACGAACAAACT	AGTTTGTTCGTTTAGATTAAAACAACACGAACGTC
28271 deletion	GAACAAACTAAATGTCTGATAATGGACCCC	GGGGTCCATTATCAGACATTTAGTTTGTTC
A28461G	CATGGCAAGGAAGGCCTTAAATTCCCTC	GAGGGAATTTAAGGCCTTCCTTGCCATG
G28881T	TCCAGGCAGCAGTATGGGAACTTCTCCTGC	GCAGGAGAAGTTCCCATACTGCTGCCTGGA
G29402T/G29427A	GCTTATGAAACTCAAGCCTTACCGCAGAAACAGAAGAAAC	GTTTCTGCGGTAAGGCTTGAGTTTCATAAGCCTTCTTCTT
G29742T/C29762T	CACTCGGAGTACGATCGAGTGTATAGTGAACAAT	ACTATACACTCGATCGTACTCCGAGTGGCCTCGG
Delta-F123-F1	cattatacgaagttatattcgatgcggccgctaatacgactcactatagattaaag	gggccgacaacatgaagacagtg
Delta-F123-F2	acactgtcttcatgttgtcggcccaaatgttaacaaag	aggtcgactctagaggatcccacATCGAtggtctcaaaggcttcagtagtatctttagc
Delta-F4	cctcttacaacagcagccaaact	caaaacactctacacgagcac
Delta-F567	tatacgaagttatattcgatgcggccgcgtctcagagtgcttttggtttatgataataag	caaacatgagaattggtcgacggccc
Delta-backbone-F567-F1	tatacgaagttatattcgatgcggccgcgtctcagagtgcttttggtttatgataataag	cttttgttgtataaacccacaaatg
Delta-backbone-F567-F2	catttgtgggtttatacaacaaaag	caatcaagccagctataaaacc
Delta-backbone-F567-F3	ggttttatagctggcttgattg	cgaggcttcttagaagcctca
RT-PCR for Sanger sequencing	**Forward primer**	**Reverse primer**
Delta vs Delta-P681	tccacttttaagtgttatggag	gttaaagcacggtttaattgtg
Delta-P681 vs Alpha	tccacttttaagtgttatggag	gttaaagcacggtttaattgtg
Delta vs Alpha	tccacttttaagtgttatggag	gttaaagcacggtttaattgtg
Alpha vs Alpha-spike/Delta-backbone	tgtagaaaacccagatatatt	tggaaaaccagctgatttgtc
Delta vs Alpha-spike/Delta-backbone	tccacttttaagtgttatggag	gttaaagcacggtttaattgtg
RT-PCR for NGS	**Forward primer**	**Reverse primer**
Delta vs Alpha	ggttttaattgttactttcctttaca	aagaacacctgtgcctgtt
Alpha vs Alpha-spike/Delta-backbone	acagtgttcccacctacaagt	ccagaagcagcgtgcatagc
Delta vs Alpha-spike/Delta-backbone	ggttttaattgttactttcctttaca	aagaacacctgtgcctgtt
Sanger sequencing	**Forward primer**	
Delta vs Delta-P681	aggatgttaactgcacaga	
Delta-P681 vs Alpha	aggatgttaactgcacaga	
Delta vs Alpha	gattgctgattataattata	
Alpha vs Alpha-spike/Delta-backbone	gttgacactgacttaacaaagcc	
Delta vs Alpha-spike/Delta-backbone	gattgctgattataattata	

Extended Data Table 2. The input and output viral RNA ratios in competition assays detected by sanger sequencing.

Groups	HAE			Calu-3		
	Days	Input ratio	Output ratio	Hours	Input ratio	Output ratio
Delta vs Alpha	Day 1	1.24	2.10	24h	1.53	4.56
	Day 2	1.24	3.24	36h	1.53	10.65
	Day 3	1.24	3.17	48h	1.53	6.21
	Day 4	1.24	3.51			
	Day 5	1.24	3.78			
Delta vs Alpha-spike/Delta-backbone	Day 1	1.07	2.97			
	Day 2	1.07	6.93			
	Day 3	1.07	10.60			
	Day 4	1.07	9.64			
	Day 5	1.07	10.53			
Alpha vs Alpha-spike/Delta-backbone	Day 1	1.45	0.59			
	Day 2	1.45	0.46			
	Day 3	1.45	0.28			
	Day 4	1.45	0.22			
	Day 5	1.45	0.15			
Delta vs Delta-P681	Day 1	0.95	2.05			
	Day 2	0.95	2.20			
	Day 3	0.95	2.38			
	Day 4	0.95	2.77			
	Day 5	0.95	3.25			
Alpha vs Delta-P681	Day 1	1.51	1.33			
	Day 2	1.51	1.13			
	Day 3	1.51	1.21			
	Day 4	1.51	0.97			
	Day 5	1.51	0.85			